

# Strong and electroweak corrections to the production of Higgs+2jets via weak interactions at the LHC

M. Ciccolini,<sup>1</sup> A. Denner,<sup>1</sup> and S. Dittmaier<sup>2</sup>

<sup>1</sup>*Paul Scherrer Institut, Würenlingen und Villigen, CH-5232 Villigen PSI, Switzerland*

<sup>2</sup>*Max-Planck-Institut für Physik (Werner-Heisenberg-Institut), D-80805 München, Germany*

(Dated: November 2, 2018)

Radiative corrections of strong and electroweak interactions are presented at next-to-leading order for the production of a Higgs boson plus two hard jets via weak interactions at the LHC. The calculation includes all weak-boson fusion and quark–antiquark annihilation diagrams as well as the corresponding interferences. The electroweak corrections, which are discussed here for the first time, reduce the cross sections by 5%, and thus are of the same order of magnitude as the QCD corrections. As argued in previous papers, where  $s$ -channel diagrams and interferences were neglected, the QCD corrections connected to interference effects are small.

PACS numbers: 12.15.Lk,13.40.Ks,13.85.-t,14.80.Bn

## INTRODUCTION

The production of a standard Higgs boson in association with two hard jets is a cornerstone in the Higgs search both in the ATLAS [1] and CMS [2] experiments at the LHC for the Higgs mass range between 100 and 200 GeV, which is favoured by the global Standard Model fit to electroweak (EW) precision data.

The production of Higgs+2jets receives two kinds of contributions at hadron colliders. The first type, where the Higgs boson couples to a weak boson that links two quark lines, is dominated by squared  $t$ - and  $u$ -channel-like diagrams and known as the “vector-boson fusion” (VBF) channel. The hard jet pairs have a strong tendency to be forward–backward directed in contrast to other jet production mechanisms, offering a good background suppression (transverse-momentum and rapidity cuts on jets, jet rapidity gap, central-jet veto, etc.). Upon applying appropriate event selection criteria (see e.g. Refs. [3, 4, 5, 6, 7] and Refs. [8, 9] for more references) it is possible to sufficiently suppress background and to enhance the VBF channel over the second H+2jets mechanism that mainly proceeds via strong interactions. In this second channel the Higgs boson is radiated off a heavy-quark loop that couples to any parton of the incoming hadrons via gluons [10, 11]. According to a recent estimate [12] hadronic production contributes about 4–5% to the Higgs+2jets events for a Higgs mass of 120 GeV after applying VBF cuts. A next-to-leading order (NLO) analysis [11] of this contribution shows that its residual scale dependence is still of the order of 35%.

Higgs production in the VBF channel is a pure EW process in leading order (LO) involving only quark and antiquark parton distributions. Approximating the cross section by  $t$ - and  $u$ -channel diagrams only (without interference), because  $s$ -channel diagrams and interferences are rather suppressed, the corresponding NLO QCD corrections reduce to vertex corrections to the weak-boson–quark coupling. Explicit NLO QCD calculations in this

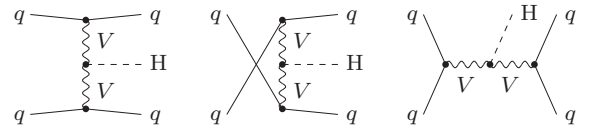


FIG. 1: Topologies for  $t$ -,  $u$ -, and  $s$ -channel contributions to  $qq \rightarrow qqH$  in LO, where  $q$  denotes any quark or antiquark and  $V$  stands for W and Z bosons.

approximation [9, 13, 14, 15, 16] confirm the expectation that these QCD corrections are quite small, because they are shifted to the parton distribution functions (PDF) via QCD factorization to a large extent. The resulting QCD corrections are of the order of 5–10% and reduce the remaining factorization and renormalization scale dependence of the NLO cross section to a few per cent.

In this paper we complete the previous NLO calculations for the VBF channel in two respects. Firstly, we add the complete NLO EW corrections, and secondly we include all interferences in the QCD corrections. While all interferences are negligibly small, as expected, the EW corrections are of the same size as the QCD corrections and thus phenomenologically relevant.

## DETAILS OF THE NLO CALCULATION

At LO, the production of Higgs+2jets via weak bosons receives contributions from the partonic processes  $qq \rightarrow Hqq$ ,  $q\bar{q} \rightarrow Hq\bar{q}$ ,  $\bar{q}q \rightarrow H\bar{q}q$ . For each relevant configuration of external quark flavours one or two of the topologies shown in Figure 1 contribute. All LO and one-loop NLO diagrams are related by crossing symmetry to the corresponding decay amplitude  $H \rightarrow q\bar{q}q\bar{q}$ . The QCD and EW NLO corrections to these decays were discussed in detail in Refs. [17, 18], in particular a representative set of Feynman diagrams can be found there.

Evaluating  $2 \rightarrow 3$  particle processes at the NLO level is non-trivial, both in the analytical and numerical parts of

the calculation. In order to ensure the correctness of our results we have evaluated each ingredient twice, resulting in two completely independent computer codes yielding results in mutual agreement. The phase-space integration is performed using multi-channel Monte Carlo techniques [19] implemented in different ways in the two different generators.

### Virtual corrections

The virtual corrections modify the partonic processes that are already present at LO; there are about 200 EW one-loop diagrams per tree diagram in each flavour channel. At NLO these corrections are induced by self-energy, vertex, box (4-point), and pentagon (5-point) diagrams. The calculation of the one-loop diagrams has been performed in the conventional 't Hooft–Feynman gauge and in the background-field formalism using the conventions of Refs. [20] and [21], respectively. The masses of the external fermions have been neglected whenever possible, i.e. everywhere but in the mass-singular logarithms.

In the  $s$ -channel diagrams intermediate W and Z bosons can become resonant, corresponding to WH/ZH production with subsequent gauge-boson decay. In order to consistently include these resonances, we implement the finite widths of the gauge bosons in the “complex-mass scheme”, which was introduced in Ref. [22] for LO calculations and generalized to the one-loop level in Ref. [23]. In this approach the W- and Z-boson masses are consistently considered as complex quantities, defined as the locations of the propagator poles in the complex plane. The scheme fully respects all relations that follow from gauge invariance.

The amplitudes have been generated with *FeynArts*, using the two independent versions 1 [24] and 3 [25]. The algebraic evaluation has been performed in two completely independent ways. One calculation is based on the in-house *Mathematica* program that was already used in the algebraic reduction of NLO corrections to the  $H \rightarrow 4$  fermions decays [17, 18]. The other has been completed with the help of *FormCalc* [26].

The tensor integrals are evaluated as in the calculation of the corrections to  $e^+e^- \rightarrow 4$  fermions [23, 27]. They are recursively reduced to master integrals at the numerical level. The scalar master integrals are evaluated for complex masses using the methods and results of Refs. [28, 29, 30]. Tensor and scalar 5-point functions are directly expressed in terms of 4-point integrals [31]. Tensor 4-point and 3-point integrals are reduced to scalar integrals with the Passarino–Veltman algorithm [32] as long as no small Gram determinant appears in the reduction. If small Gram determinants occur, the alternative schemes described in Ref. [33] are applied.

### Real corrections

Real QCD corrections consist of gluon emission and processes with  $gq$  and  $g\bar{q}$  initial states. Analogously real photonic corrections comprise photon bremsstrahlung and photon-induced processes with  $\gamma q$  and  $\gamma\bar{q}$  initial states. The matrix elements for these corrections have been evaluated using the Weyl–van der Waerden spinor technique as formulated in Ref. [34] and have been checked against results obtained with *Madgraph* [35].

All types of real corrections involve singularities from collinear initial-state splittings which are regularized with small quark masses. The mass singularities are absorbed via factorization by the usual PDF redefinition both for the QCD and photonic corrections (see, e.g., Ref. [36]). Technically, the soft and collinear singularities for real gluon or photon emission are isolated both in the dipole subtraction method following Ref. [37] and in the phase-space slicing method. For gluons or photons in the initial state the subtraction and slicing variants described in Ref. [36] are applied. The results presented in the following are obtained with the subtraction method, which numerically performs better.

## NUMERICAL RESULTS

We use the input parameters as given in Ref. [17]. Since quark-mixing effects are suppressed, we set the CKM matrix to the unit matrix. The electromagnetic coupling is fixed in the  $G_\mu$  scheme, i.e. it is set to  $\alpha_{G_\mu} = \sqrt{2}G_\mu M_W^2 s_w^2 / \pi$ , because this accounts for electromagnetic running effects and some universal corrections of the  $\rho$  parameter.

We use the MRST2004QED PDF [38] which consistently include  $\mathcal{O}(\alpha)$  QED corrections. These PDF include a photon distribution function for the proton and thus allow to take into account photon-induced partonic processes. As explained in Ref. [36], the consistent use of these PDF requires the  $\overline{\text{MS}}$  factorization scheme for the QCD, but the DIS scheme for the QED corrections; the corresponding factorization scales are identified with the Higgs mass  $M_H$  if not stated otherwise. We only use four quark flavours for the initial partons, i.e. we do not take into account the contribution of bottom quarks, which is suppressed. Since no associated LO version of the MRST2004QED PDF exists, we use these PDF both for LO and NLO predictions. For the renormalization scale of the strong coupling constant by default we employ  $M_H$ , include 5 flavours in the two-loop running, and fix  $\alpha_s(M_Z) = 0.1187$ .

Apart from the total cross section without any phase-space cuts, we consider the integrated cross section defined after applying typical VBF cuts to the outgoing jets. In this case, jets are defined from partons using the  $k_T$ -algorithm [39, 40, 41] as described in Ref. [42].

More precisely, jets result from partons of pseudorapidity  $|\eta| < 5$  using the jet resolution parameter  $D = 0.8$ . We also recombine real photons with partons or jets according to this algorithm. Thus, some of the photons end up in jets, others are left as identifiable photons. Following Ref. [15], we specify the VBF cuts as follows. We require at least two hard jets with

$$p_{Tj} \geq 20 \text{ GeV}, \quad |y_j| \leq 4.5, \quad (1)$$

where  $p_{Tj}$  is the transverse momentum of the jet and  $y_j$  its rapidity. The tagging jets  $j_1$  and  $j_2$  are then defined as the two jets passing the cuts (1) with highest  $p_T$  and  $p_{Tj_1} > p_{Tj_2}$ . Finally, we demand a large rapidity separation of the two tagging jets by

$$\Delta y_{jj} \equiv |y_{j_1} - y_{j_2}| > 4, \quad y_{j_1} \cdot y_{j_2} < 0. \quad (2)$$

In Figure 2 we plot the total cross section with and without cuts as a function of  $M_H$ . In the upper panel we show the absolute predictions in LO and in NLO including QCD and EW corrections. The VBF cuts reduce the cross section by a factor 3–4. In the lower panel we show the relative corrections. Without cuts the QCD corrections are about +5% and the EW corrections about –5% both depending only weakly on  $M_H$  and cancelling each other substantially. With cuts the EW corrections are approximately –6%, while the QCD corrections vary between –3% and +2%. In the EW corrections the WW and ZZ thresholds are clearly visible. It is interesting to note that the EW corrections to the full VBF channel are similar in size and sign to the EW corrections to the subreactions  $pp \rightarrow WH/ZH + X$  [43]. Compared to the related decays the  $H \rightarrow WW/ZZ \rightarrow 4f$  [17, 18] the size is similar, but the sign is different.

In Table I we present integrated cross sections for  $M_H = 120, 150, 170,$  and  $200 \text{ GeV}$  without any cuts and in Table II results for VBF cuts. We list the LO cross section  $\sigma_{LO}$ , the cross section  $\sigma_{NLO}$  including QCD+EW corrections, and the relative QCD and EW corrections,  $\delta_{QCD}$  and  $\delta_{EW}$ , respectively. The complete EW corrections  $\delta_{EW}$  also comprise the corrections from photon-induced processes  $\delta_{\gamma\text{-induced}}$ , which turn out to be  $\sim +1\%$  and to reduce the EW corrections. We note that the QCD corrections are dominated by the known (vertex-like) corrections to the squared  $t$ - and  $u$ -channel VBF diagrams, while corrections to interference terms are at the level of 0.1%. These interference corrections are not enhanced by contributions of two  $t$ - or  $u$ -channel vector bosons with small virtuality and therefore even further suppressed when applying VBF cuts.

In Figure 3 we show the dependence of the total cross section on the factorization and renormalization scale for  $M_H = 120 \text{ GeV}$ . We set the factorization scale  $\mu \equiv \mu_F$ , which applies to both QCD and QED contributions, equal to the renormalization scale  $\mu_R = \mu$  and vary it between  $M_H/8$  and  $8M_H$ . In this set-up, we show the

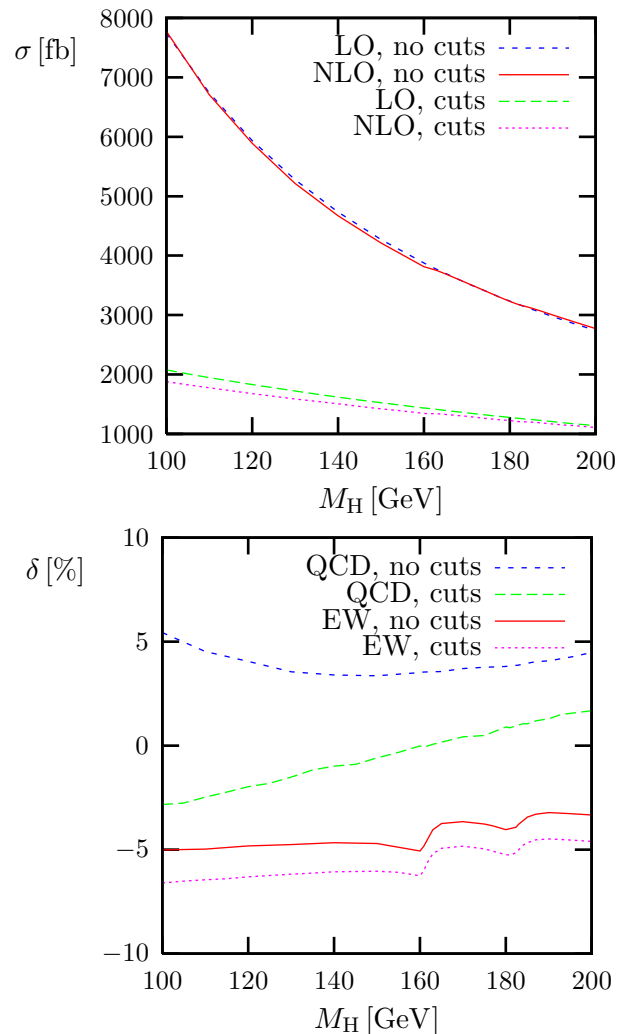


FIG. 2: Higgs mass dependence of LO and complete NLO cross section (upper) and relative EW and QCD corrections (lower) without and with VBF cuts.

$M_H$ [GeV]	120	150	170	200
$\sigma_{LO}$ [fb]	5936(1)	4271(2)	3536(1)	2743(1)
$\sigma_{NLO}$ [fb]	5890(2)	4219(2)	3538(1)	2775(1)
$\delta_{QCD}$ [%]	4.04(3)	3.47(2)	3.72(2)	4.48(2)
$\delta_{EW}$ [%]	-4.81(2)	-4.70(2)	-3.65(1)	-3.33(1)
$\delta_{\gamma\text{-induced}}$ [%]	0.86(1)	1.04(1)	1.14(1)	1.27(1)

TABLE I: Cross section for  $pp \rightarrow H + 2\text{jets} + X$  in LO and NLO without cuts and relative QCD and EW corrections. The contribution  $\delta_{\gamma\text{-induced}}$  from  $\gamma$ -induced processes (which is part of  $\delta_{EW}$ ) is also given separately.

$M_H$ [GeV]	120	150	170	200
$\sigma_{LO}$ [fb]	1830.5(5)	1524.2(4)	1353.8(3)	1139.1(3)
$\sigma_{NLO}$ [fb]	1678.7(9)	1422.9(7)	1293.4(6)	1106.0(5)
$\delta_{QCD}$ [%]	-1.97(4)	-0.60(4)	0.41(4)	1.76(3)
$\delta_{EW}$ [%]	-6.32(2)	-6.02(2)	-4.87(1)	-4.64(1)
$\delta_{\gamma\text{-induced}}$ [%]	1.14(1)	1.21(1)	1.25(1)	1.31(1)

TABLE II: As in Table I, but with VBF cuts applied.

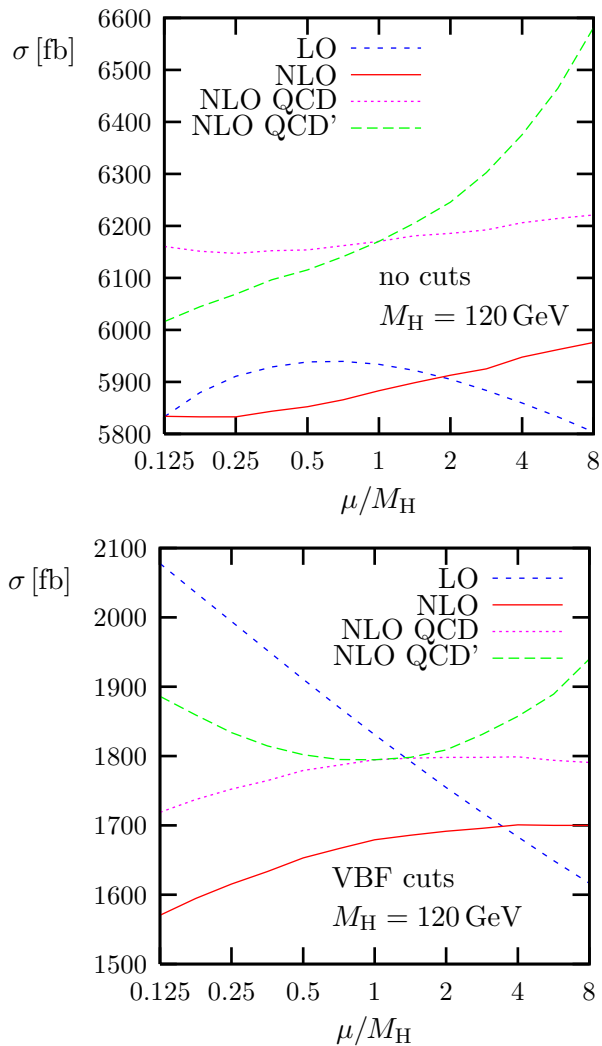


FIG. 3: Scale dependence of LO and NLO cross sections with QCD or QCD+EW corrections for  $M_H = 120$  GeV without cuts (upper) and with VBF cuts (lower),  $\mu_R = \mu_F \equiv \mu$  for LO, NLO and NLO QCD, but  $\mu_R = M_H^2/\mu$  for NLO QCD'.

LO cross section, the QCD corrected NLO cross section and the complete NLO cross section involving both QCD and EW corrections. In addition we depict the QCD corrected NLO cross section for the setup where  $\mu_R = M_H^2/\mu$  (NLO QCD'). Varying the scale  $\mu$  up and down by a factor 2 (8) changes the cross section by 11% (29%) in LO and 3% (18%) in NLO for the set-up with VBF cuts. Without cuts the scale uncertainty it is at the level of 3% (11%) in NLO, while it is accidentally small in LO for this specific Higgs-boson mass.

## CONCLUSIONS

Radiative corrections of strong and electroweak interactions have been discussed at next-to-leading order for Higgs production via vector-boson fusion at the LHC. The electroweak corrections, which have not been cal-

culated before, reduce the cross section by 5%, and are thus as important as the QCD corrections in this channel. QCD corrections to interference contributions turn out to be negligible, confirming previous approximations.

Acknowledgement: This work is supported in part by the European Community's Marie-Curie Research Training Network HEPTOOLS under contract MRTN-CT-2006-035505. We thank M. Spira for comments on the manuscript.

- 
- [1] S. Asai et al., Eur. Phys. J. **C32S2**, 19 (2004), hep-ph/0402254.
  - [2] S. Abdullin et al., Eur. Phys. J. **C39S2**, 41 (2005).
  - [3] V. Del Duca et al., JHEP **10**, 016 (2006), hep-ph/0608158.
  - [4] V. D. Barger, R. J. N. Phillips, and D. Zeppenfeld, Phys. Lett. **B346**, 106 (1995), hep-ph/9412276.
  - [5] D. L. Rainwater and D. Zeppenfeld, JHEP **12**, 005 (1997), hep-ph/9712271.
  - [6] D. L. Rainwater, D. Zeppenfeld, and K. Hagiwara, Phys. Rev. **D59**, 014037 (1999), hep-ph/9808468.
  - [7] D. L. Rainwater and D. Zeppenfeld, Phys. Rev. **D60**, 113004 (1999), hep-ph/9906218.
  - [8] A. Djouadi (2005), hep-ph/0503172.
  - [9] M. Spira, Fortsch. Phys. **46**, 203 (1998), hep-ph/9705337.
  - [10] V. Del Duca et al., Nucl. Phys. **B616**, 367 (2001), hep-ph/0108030.
  - [11] J. M. Campbell, R. Keith Ellis, and G. Zanderighi, JHEP **10**, 028 (2006), hep-ph/0608194.
  - [12] M. V. Acosta and A. Nikitenko (2007), arXiv:0705.3585 [hep-ph].
  - [13] T. Han, G. Valencia, and S. Willenbrock, Phys. Rev. Lett. **69**, 3274 (1992), hep-ph/9206246.
  - [14] T. Figy, C. Oleari, and D. Zeppenfeld, Phys. Rev. **D68**, 073005 (2003), hep-ph/0306109.
  - [15] T. Figy and D. Zeppenfeld, Phys. Lett. **B591**, 297 (2004), hep-ph/0403297.
  - [16] E. L. Berger and J. Campbell, Phys. Rev. **D70**, 073011 (2004), hep-ph/0403194.
  - [17] A. Bredenstein, A. Denner, S. Dittmaier, and M. M. Weber, Phys. Rev. **D74**, 013004 (2006), hep-ph/0604011.
  - [18] A. Bredenstein, A. Denner, S. Dittmaier, and M. M. Weber, JHEP **02**, 080 (2007), hep-ph/0611234.
  - [19] J. Hilgart, R. Kleiss, and F. Le Diberder, Comput. Phys. Commun. **75**, 191 (1993).
  - [20] A. Denner, Fortsch. Phys. **41**, 307 (1993).
  - [21] A. Denner, S. Dittmaier, and G. Weiglein, Nucl. Phys. **B440**, 95 (1995), hep-ph/9410338.
  - [22] A. Denner, S. Dittmaier, M. Roth, and D. Wackerroth, Nucl. Phys. **B560**, 33 (1999), hep-ph/9904472.
  - [23] A. Denner, S. Dittmaier, M. Roth, and L. H. Wieders, Nucl. Phys. **B724**, 247 (2005), hep-ph/0505042.
  - [24] J. Küblbeck, M. Böhm, and A. Denner, Comput. Phys. Commun. **60**, 165 (1990).
  - [25] T. Hahn, Comput. Phys. Commun. **140**, 418 (2001), hep-ph/0012260.
  - [26] T. Hahn and M. Perez-Victoria, Comput. Phys. Commun. **118**, 153 (1999), hep-ph/9807565.

- [27] A. Denner, S. Dittmaier, M. Roth, and L. H. Wieders, Phys. Lett. **B612**, 223 (2005), hep-ph/0502063.
- [28] A. Denner, U. Nierste, and R. Scharf, Nucl. Phys. **B367**, 637 (1991).
- [29] G. 't Hooft and M. J. G. Veltman, Nucl. Phys. **B153**, 365 (1979).
- [30] W. Beenakker and A. Denner, Nucl. Phys. **B338**, 349 (1990).
- [31] A. Denner and S. Dittmaier, Nucl. Phys. **B658**, 175 (2003), hep-ph/0212259.
- [32] G. Passarino and M. J. G. Veltman, Nucl. Phys. **B160**, 151 (1979).
- [33] A. Denner and S. Dittmaier, Nucl. Phys. **B734**, 62 (2006), hep-ph/0509141.
- [34] S. Dittmaier, Phys. Rev. **D59**, 016007 (1999), hep-ph/9805445.
- [35] T. Stelzer and W. Long, Comput. Phys. Commun. **81**, 357 (1994), hep-ph/9401258.
- [36] K. P. O. Diener, S. Dittmaier, and W. Hollik, Phys. Rev. **D72**, 093002 (2005), hep-ph/0509084.
- [37] S. Dittmaier, Nucl. Phys. **B565**, 69 (2000), hep-ph/9904440.
- [38] A. D. Martin, R. G. Roberts, W. J. Stirling, and R. S. Thorne, Eur. Phys. J. **C39**, 155 (2005), hep-ph/0411040.
- [39] S. Catani, Y. L. Dokshitzer, and B. R. Webber, Phys. Lett. **B285**, 291 (1992).
- [40] S. Catani, Y. L. Dokshitzer, M. H. Seymour, and B. R. Webber, Nucl. Phys. **B406**, 187 (1993).
- [41] S. D. Ellis and D. E. Soper, Phys. Rev. **D48**, 3160 (1993), hep-ph/9305266.
- [42] G. C. Blazey et al. (2000), hep-ex/0005012.
- [43] M. L. Ciccolini, S. Dittmaier, and M. Krämer, Phys. Rev. **D68**, 073003 (2003), hep-ph/0306234.